ELSEVIER

Journal of Fluids and Structures 26 (2010) 41–49

JOURNAL OF FLUIDS AND STRUCTURES

www.elsevier.com/locate/jfs

On the wake of a circular cylinder with nodal and saddle attachment

Anwar Ahmed*

Aerospace Engineering Department, Auburn University, Auburn, AL 36849, USA

Received 18 July 2008; accepted 17 September 2009
Available online 28 October 2009

Abstract

Flow field of a cylinder with a mid-span curvature was experimentally investigated in a wind tunnel and a water tunnel. The azimuthal orientation of the cylinder was changed to obtain a nodal, saddle and a mixed nodal–saddle type of flow attachment. Surface flow topology suggested that the nature of the attachment strongly influenced the spanwise distributions of foci structures that play a significant role in introducing three-dimensionality in the immediate wake. Flow visualization in the water tunnel revealed that the length of a vortex formation region also followed the changes in the nature of the attachment. A symmetric shedding of vortices was observed with a saddle type of attachment. Wake mean velocity profiles showed that the velocity defect and therefore the drag of a curved cylinder was minimum for nodal, and maximum for saddle type of attachment. Nomenclature of the wake was compared with asymptotic profiles and equilibrium parameters. Approach to self-preservation, similarity and other features are discussed.

Keywords: Curved cylinder; Equilibrium wakes; Three-dimensional attachment

1. Introduction

Towing cables, stranded wires and other flexible structural elements in airborne and offshore marine applications are subjected to flow-induced vibrations and unsteady wakes that cause structural fatigue and often result in unpredictable failures. Relf and Powell (1917) were the first to report tests on flexible cables, followed by McLeod (1918). Analytical treatment of the problem posed by towed cables was first reported by Philips (1949) who noted that a towed body subjected to cable-induced oscillations experiences stability problems such as longitudinal whipping. These problems, however, are largely rooted in the resonant unsteady fluid and elastic coupling that occurs due to a combination of bluff body oscillations (Bearman, 1984), spanwise cellular breakdown of symmetry due to attachment line shape (Ahmed and Bays-Muchmore, 1992; Ahmed et al., 1993; Darekar and Sherwin, 2001; Owen et al., 2001), orientation (Ramberg, 1983), etc. Two-dimensional bluff body wakes and free shear layers contain spanwise deterministic coherent structures such as the Karman vortices (e.g., see Roshko, 1954; Gerrard, 1978) and rollers (e.g., see Lasheras and Choi, 1988; Meiburg and Lasheras, 1988). Smaller scale quasi-deterministic structures such as streamwise vortices have been observed by several researchers in the past, notably Townsend (1979) and Wei and Smith (1986). These smaller scales that are in the form of streamwise vortices,

*Corresponding author. Tel.: +1 334 844 6817; fax: +1 334 844 6803.
E-mail address: aahmed@eng.auburn.edu

0889-9746/$ - see front matter © 2009 Elsevier Ltd. All rights reserved.
doi:10.1016/j.jfluidstructs.2009.09.002

Nomenclature

b	half wake width
D	cylinder diameter
f	vortex shedding frequency
U	mean axial velocity
U_o	edge velocity
U_∞	free-stream velocity
St	Strouhal number, fD/U
Re	Reynolds number, UD/v
W	wake velocity deficit (W_o, centerline defect)
X,Y,Z	streamwise, transverse and spanwise coordinates
θ	momentum thickness
v	kinematic viscosity
φ	flow attachment angle, measured clockwise from the direction of free-stream flow

however, extract energy from larger coherent structures and significantly distort the wake and introduce three-dimensionality that continues to increase as the flow continues downstream (Hayakawa and Hussain, 1989). Although, considered to be a route to transition in the wake, streamwise vortices have been observed in fully turbulent wakes as well (Bays-Muchmore and Ahmed, 1993). Hama (1957) has addressed in detail the three-dimensionality of the cylinder wake that is also vividly seen in the flow visualization results of Gerrard (1978) who reported the presence of ''knots'' and ''fingers'' superimposed on the von Karman vortices in the wake. Flow over a right circular cylinder therefore is an example of degenerate topological flow, as any three-dimensionality introduced into such a domain causes bifurcation of the flow to a stable topology of nodes and saddles, as described by Dallmann and Schewe (1987). Two-dimensionality therefore exists only as an idealization. In practice, three-dimensional effects are always present. Williamson (1996), for example, has stressed the role of end conditions in the spread of three-dimensionality in the wake and if the cylinder geometry does not determine their form, it is determined by uncontrolled factors such as small perturbations in the incident-free stream. These uncontrolled structures move in space making them difficult to study.

The flow field of a yawed cylinder is significantly different from that of right circular cylinders, due to the nature of boundary layer and pressure distribution discussed in detail by Sears (1948). Because of the cross-stream pressure gradients, the base pressure and flow characteristics show higher sensitivity to the asymmetric end-wall conditions and the wake is essentially unsteady and three-dimensional (e.g., see Ramberg and Griffin, 1976; Shirakashi et al., 1986). With the exception of tow tanks, much of the experimental work in the wind tunnels has been modeled by yawed cylinders in cross-flow (Bursnall and Loftin, 1951). Finite length cylindrical bodies at incidence on the other hand produce multiple vortices in the wake (Thomson and Morrison, 1971).

In practice a tethered flexible cable has a finite curvature due to weight and end conditions and therefore the oncoming flow is not perfectly normal to its axis. The resulting curved attachment line can impose additional strain on the flow and can vary along the entire length as the radius of curvature changes. The attachment line flow further depends on the azimuthal orientation and also serves as the source of three-dimensionality in the wake that can either attenuate or amplify the unsteady loads on a cable due to vortex shedding.

As a part of an ongoing research on vortex dynamics the primary objective of the present work was to investigate wake of a circular cylinder with mid-span curvature capable of topologically different flows along the attachment line.

2. Experimental set-up

The geometry of the curved cylinder model used in the investigation is shown in Fig. 1. The model was made from a 25 mm diameter solid acrylic rod. The overall length of the model was 40 diameters and the mid-part was smoothly bent at a radius of curvature of 20 diameters. This reduced the transverse length to 36 diameters, and the model thus spanned the entire width of the wind tunnel. Five azimuthal angles of flow attachment ($\varphi = 0^\circ, 45^\circ, 90^\circ, 135^\circ, 180^\circ$) were tested. The attachment of the flow is therefore described as nodal when $\varphi = 0^o$ and saddle when $\varphi = 180^\circ$. A 25 mm diameter straight cylinder was also tested for comparison purposes.

Wind tunnel tests were conducted in a 61 cm × 92 cm closed circuit wind tunnel equipped with a two-degree-of-freedom traversing system. Total pressures in the wake were measured with the help of a Kiel probe connected to a Valedyne DP45-14 pressure transducer. The test Reynolds number based of cylinder diameter was 20 000. Wake power spectra were measured with the help of a Dantec single wire probe connected to a Dantec 56C17 Bridge, 56N21 Linearizer and a 56N20 Signal Conditioner. Data was acquired at 20 kHz on a PC and post processed using Matlab software. A HP 3563A System Analyzer was also used to determine primary shedding frequency during the tests.

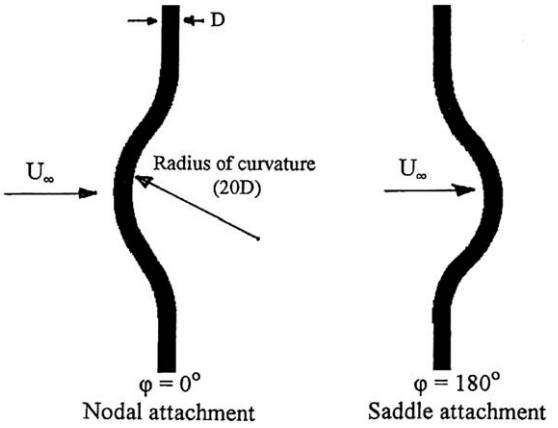

Fig. 1. Model geometry and description of azimuthal attachment angle φ.

A unique technique was employed for cylinder surface flow visualization in the wind tunnel. It consisted of covering the entire cylinder with shrink-wrap tubing coated with tempera powder mixed with kerosene oil and oleic acid. After the oil evaporated at a given test condition, the wrapped tubing was longitudinally cut from the rear with a sharp knife and straightened like a processed snake skin. The "skin" was later sprayed with transparent acrylic and photographed to obtain permanent record of the limiting streamlines. The wake of the curved cylinder was visualized in a 61 cm × 92 cm cross-section water tunnel at Reynolds numbers of 1300. A 0.127 mm platinum wire was used to produce pulsed and continuous hydrogen bubble sheets. A 4 W Argon-ion laser beam was used to form a light sheet to illuminate the bubbles in various planes of interest. Video images from a NEC T123A CCD camera were recorded on a Toshiba SV-F990 VCR. Video records were analyzed frame by frame and selected images were printed on a Sony thermal printer.

3. Results and discussion

3.1. Flow visualization

3.1.1. Wind tunnel flow visualization

Surface flow visualization in the wind tunnel provided a new insight into the origin of the structures present in the cylinder wake as observed in the water tunnel for different azimuthal attachment of the flow. In order to show the limiting streamlines clearly and to prevent wrinkling, the shrink wrap for the $\varphi = 0^\circ$ case was cut just under the attachment line, and for the $\varphi = 180^\circ$ case it was cut from the rear. Surface flow visualization results presented in Fig. 2 for nodal and saddle attachment show the primary separation lines, secondary separation lines and foci structures. Foci structures are classified as unstable limit cycles whereby the dye from outside accumulates towards the center and leaves the surface (Maskel, 1955; Perry and Fairlie, 1974).

Azimuthal locations of primary separation lines on straight cylinders for fully turbulent flows have been reported to be at 116° by Roshko (1961) and 115° by Achenbach (1968). The laminar separation, on the other hand, occurs ahead of 90° as the surface pressure begins to rise. The measured locations of the primary separation lines for the cases tested were well below the turbulent values, and also because of the low Reynolds number, it was concluded that the separation was laminar. The locations of primary separation lines as measured from the attachment line was at $\pm 80^\circ$ for $\varphi = 0^\circ$ and moved upstream to $\pm 73^\circ$ for $\varphi = 180^\circ$ case and are labeled in Fig. 2. Similarly the secondary separation lines were located at $\pm 145^\circ$ for $\varphi = 0^\circ$ and moved downstream to $\pm 152^\circ$ for $\varphi = 180^\circ$ case. In comparison, the primary and secondary separation lines for the straight cylinder were at $\pm 80^\circ$ and $\pm 170^\circ$, respectively.

For nodal attachment ($\varphi = 0^\circ$), the limiting streamlines move outwards spanwise and after traversing the circumference converge to form foci between the primary and secondary separation lines on the leeward side. The flow later detaches at foci and spirals off into the wake. These foci structures on the leeward side of the cylinder presented in Fig. 2(a) are very different from the dominant foci structures observed for a right circular cylinder by Bays-Muchmore and Ahmed (1993).

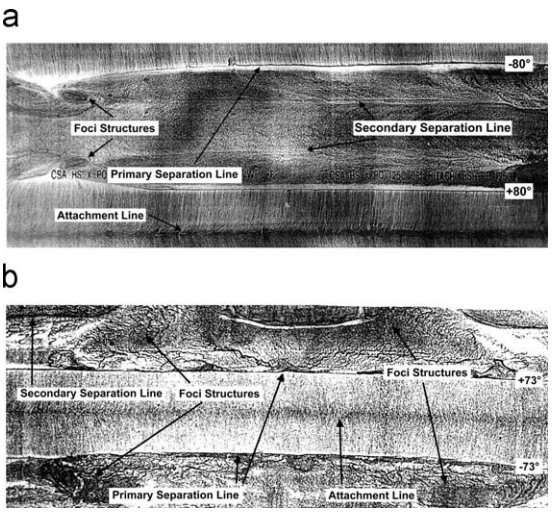

Fig. 2. Surface flow visualization of cylinder: (a) $\varphi = 0^\circ$ and (b) $\varphi = 180^\circ$.

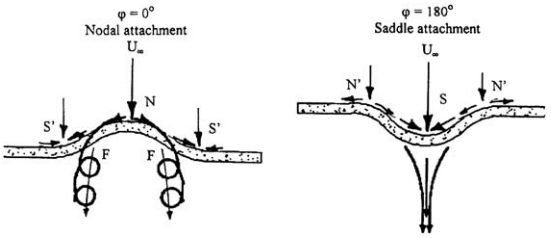

Fig. 3. Topological cartoon of flow inferred from flow visualization.

Surry (1965) in his flow visualization work with curved cylinders has reported similar results. He also reported spanwise flow to be away from the cylinder centerline and towards its ends and formation of eddies in the wake. These eddies produced narrow reverse flow channels behind the separation line, resulting in flow detaching and bleeding off from four stagnation regions into the wake. In the present investigation four foci structures were observed to occur on the leeward side of the cylinder. The location of these foci structures was different than what was observed by Surry and is attributed to differences in end-wall conditions, type of attachment and separation. For the $\varphi = 180^\circ$ case, the limiting streamlines move towards the centerline along the attachment line and intersect at the saddle where two streamlines emanate from the saddle and traverse the circumference towards the leeward side where they converge with the near surface flow to form foci structures (Fig. 2(b)).

It may be noted that the foci were displaced outwards, i.e. away from the centerline to ± 5 diameters for $\varphi = 0^\circ$ but were displaced only ± 1 diameter from the centerline for $\varphi = 180^\circ$. This indicated that the wake was narrow due to lateral stretching for nodal attachment and wider due to lateral compression for a saddle type of attachment. These observations were substantiated by water tunnel flow visualization and wake velocity surveys. A topological description the surface flow is presented in Fig. 3. Here F is focus in velocity vector field topology, N and S are nodes and saddles in shear stress field topology, and N′ and S′ are skewed singular points (Hunt et al., 1978; Tobak and Peake, 1982).

3.1.2. *Water tunnel flow visualization*

For yawed cylinders it has been noted that the end-wall conditions alter the cross-flow effects in the wake significantly. Thus, through harmonic and/or sub-harmonic coupling, the end-wall effects can amplify or attenuate certain modes that may not be the characteristic of the flow altogether. However, in the case of a curved cylinder the symmetric boundary conditions imposed symmetric strains and some unique features of the wake therefore remained intact. Results of flow visualization of curved cylinder for Reynolds number of 1300 are presented in Fig. 4. For the nodal attachment ($\varphi = 0^\circ$), von Karman vortex street is visible but is significantly distorted by additional flow structures. The side view of the same flow in Fig. 4(b) shows the curvature of the vortex street, streamwise vortices and

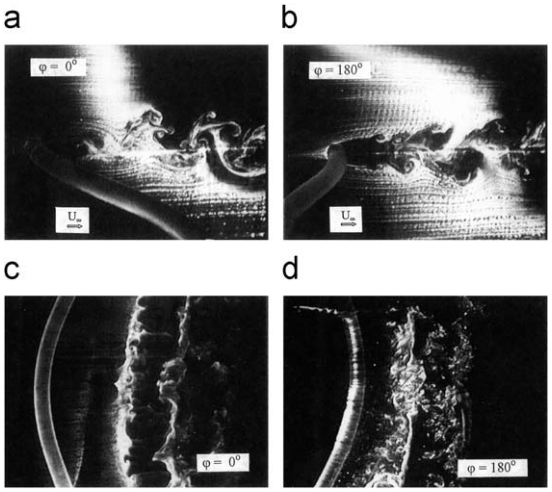

Fig. 4. Flow visualization of the cylinder wake.

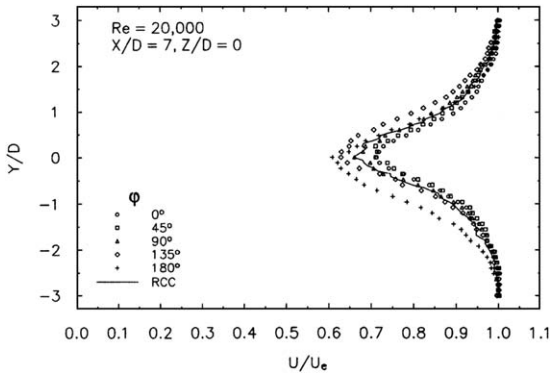

Fig. 5. Wake mean velocity profiles.

distortions. For saddle attachment ($\varphi = 180^\circ$) symmetric shedding of shear layer vortices followed by an asymmetric growth within 6 diameters is visible in Fig. 4(c). A side view of the same flow in Fig. 4(d) shows the presence of larger scales and highly three-dimensional wake.

The length of the vortex formation region was measured from video records and was found to be 1.13 diameters for the straight cylinder, 1.5 diameters for $\varphi = 0^\circ$ and steadily increased to 3 diameters for $\varphi = 180^\circ$. This shows that this length is dependent not only on Reynolds number and three-dimensionality in the wake (Williamson, 1996) but also on the attachment line geometry as previously observed by Ahmed et al. (1993).

3.2. Wake surveys

Total pressure surveys in the wake were conducted at six streamwise stations ($X/D = 3$, 5, 7, 9, 15, 20). At each station wake was traversed vertically ranging from $Y/D = \pm 3$ for the first four stations and $Y/D = \pm 6$ for the remaining two stations. Wake power spectra were measured at the edge of the wake at each station.

3.2.1. Mean velocity profiles

Fig. 5 shows the mean velocity profiles in the wake of a curved cylinder at $X/D = 7$ and in the plane of symmetry ($Z/D = 0$) for various azimuthal attachments ($\varphi = 0$–180°). The results are compared with the data of a straight cylinder. Using the momentum deficit method, the velocity defect plots were integrated to obtain the drag coefficient C_d. A $C_d = 0.8$ for nodal attachment was lower than $C_d = 0.95$ for a right circular cylinder. The value of C_d increased gradually for up to $\varphi = 90^\circ$ and increased rapidly to its maximum value of 1.15 for $\varphi = 180^\circ$.

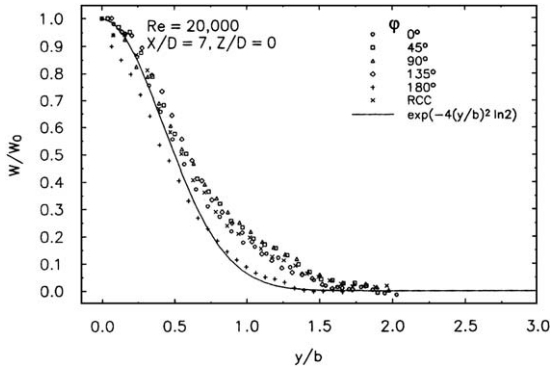

Fig. 6. Wake mean velocity defect profiles.

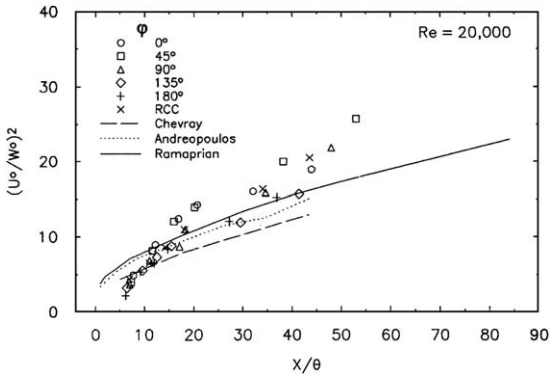

Fig. 7. Variation of W_o in the wake.

The value of the shape factor calculated from integral quantities in the wake at the last measurement station was 1.2. This indicated that self-preservation was not achieved up to 55 momentum thicknesses downstream in the wake, although the trends towards the asymptotic value were correct. Velocity defect profiles are compared with the mean asymptotic profile of Ramaprian et al. (1982) in Fig. 6 for $X/D = 20$. A slight overshoot in a region between $Y/b = 0.5$ and 1.5 is observed and is attributed to three-dimensionality of the wake.

3.2.2. *Variation of W_o and b*

A wake is supposed to have reached self-preserving state when it conforms to the following asymptotic trends suggested by Ramaprian et al. (1982):

$$W_o \propto X^{-1/2}, \quad b \propto X^{1/2},$$

where W_o is the maximum velocity defect and b is the half wake width. Results of the curved cylinder wake are compared with the straight cylinder wake, and the flat plate data of Ramaprian et al. (1982), Chevray and Kovasznay (1969) and Andreopoulos and Bradshaw (1980) in Figs. 7 and 8. Slopes were observed to be slightly higher compared to flat plate data. In the near-wake region some scatter was observed; however, linear variations were observed at higher X/θ values, indicating that the wake was approaching a self-preserving state. An increase in slopes with increasing φ was also noted. This is attributed to the appearance of additional eddies and turbulence as observed in the wakes during the flow visualization tests in the water tunnel.

Sreenivasan (1981) stated that a self-preserving wake is characterized by two parameters:

$$\left(\frac{W_o}{U}\right)\sqrt{\frac{x}{\theta}} \text{ and } \frac{b}{\sqrt{X\theta}}.$$

These equilibrium parameters attain universal values of 1.63 ± 0.02 and 0.30 ± 0.05, respectively, if the wake is self-preserving. These parameters, plotted in Figs. 9 and 10, show that, although the curved cylinder wake for nodal

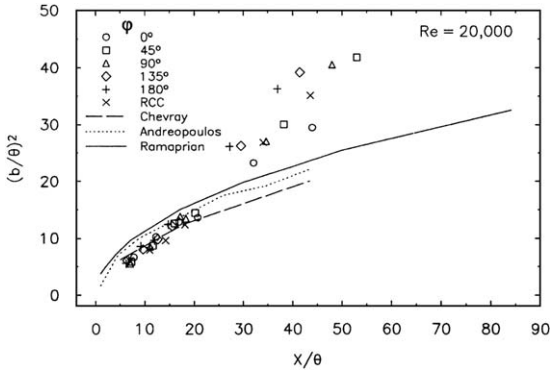

Fig. 8. Variation of wake half-width.

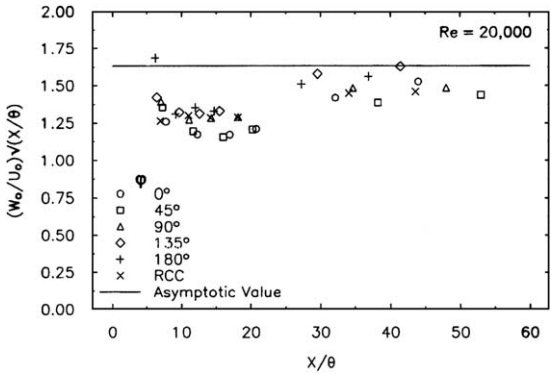

Fig. 9. Comparison of wake defect equilibrium parameter.

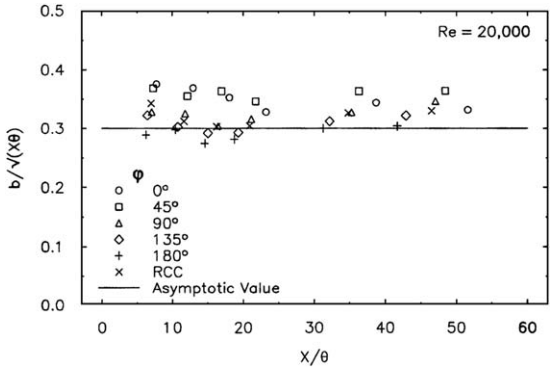

Fig. 10. Comparison of wake half-width equilibrium parameters.

attachment tends to approach these values faster than the straight cylinder wake, the wake failed to achieve equilibrium state. Another interesting aspect to note is that the route to equilibrium state appears to be highly dependent of the nature of attachment, separation and state of boundary layer.

3.2.3. *Wake power spectrum*

Unfiltered wake power spectra for the straight cylinder, $\varphi = 0^\circ$ and 180° cases, are presented in Fig. 11. In addition to higher power spectral density noted for both types of attachment compared to the straight cylinder, a shift in the fundamental shedding frequency towards higher wavenumbers for the $\varphi = 0^\circ$ case and towards lower wave numbers for

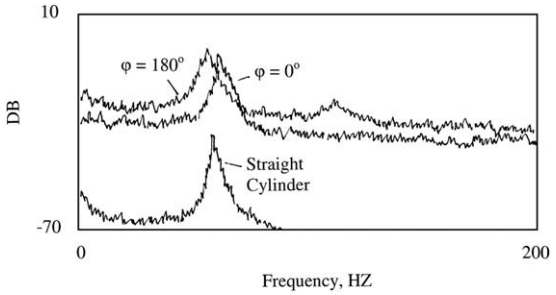

Fig. 11. Wake power spectra.

the $\varphi = 180^\circ$ case is evident. On the average this shift is ± 2.5 Hz from the fundamental shedding frequency of straight cylinder. This indicates that the wake undergoes lateral stretching due to "outward" flow for the nodal attachment and lateral compression due to "inward" flow for the saddle type of attachment. Consequently the convection velocity in the wake is increased for the nodal attachment and reduced for saddle attachment. Power spectra for the $\varphi = 0^\circ$ and 180° wakes show gradual roll-off past the shedding frequency indicating distribution of energy to additional flow structures at higher wavenumbers. However, for the $\varphi = 180^\circ$ case, the energy distribution is higher as compared to $\varphi = 0^\circ$, indicating relatively higher levels of broad-band turbulence. Both harmonic (appearance of smaller eddies) and sub-harmonic (indicative of amalgamation of fluid structures) interactions are evident for the $\varphi = 180^\circ$ case.

4. Conclusions

Counter-rotating foci structures located between primary and secondary separation lines were observed to be the dominant features of the curved cylinder wake. These foci were displaced outwards when the singular point of attachment was a node, and inwards for saddle attachment. The displacement of foci along with the direction of rotation was such that the Karman vortices were stretched for nodal attachment. The opposite was true for saddle attachment whereby the distortion of the vortex street was more pronounced and turbulent. Based on the detailed analysis of flow visualization data, it is also concluded that vortex splitting occurs when a strained vortex undergoes axial stretching. A vortex dislocation, on the other hand, occurs due to axial compression. A shift in primary shedding frequency was observed with the azimuthal orientation of the cylinder, resulting in a variation of the Strouhal number. Drag for the nodal attachment was less than for the saddle attachment due to the differences in the wake. Trends for approach to equilibrium were faster for saddle type of attachment, and this is attributed to higher turbulence and mixing in the wake.

Acknowledgment

This work was partly supported by a grant from Office of Naval Research, Contract No. N00014-93-1-10138 and through funds provided by Auburn University Office of Vice President Research Competitive Research Grant Program.

References

Achenbach, E., 1968. Distribution of local pressure and skin friction around a circular cylinder in cross-flow up to $Re = 5 \times 10^6$. Journal of Fluid Mechanics 34, 625–639.

Ahmed, A., Khan, M.J., Bays-Muchmore, B., 1993. Experimental investigation of a three-dimensional bluff body wake. AIAA Journal 31, 559–563.

Ahmed, A., Bays-Muchmore, B., 1992. Transverse flow over a wavy cylinder. Physics of Fluids A 4, 1959–1967.

Andreopoulos, J., Bradshaw, P., 1980. Measurements of interacting shear layers in the near wake of a flat plate. Journal of Fluid Mechanics 100, 639–668.

Bays-Muchmore, B., Ahmed, A., 1993. On the streamwise vortices in the turbulent wakes of cylinders. Physics of Fluids A 5, 387–392.

Bearman, P.W., 1984. Vortex shedding from oscillating bodies. Annual Review of Fluid Mechanics 16, 195–222.

Bursnall, W.J., Loftin Jr., L.K., 1951. Experimental investigation of the pressure distribution about a yawed circular cylinder in the critical Reynolds number range. NACA TN 2463.
Chevray, R., Kovasznay, L.S.G., 1969. Turbulence measurement in the wake of a thin flat plate. AIAA Journal 7, 1641–1643.
Dallmann, U., Schewe, G., 1987. On topological changes of separating flow structures at transition Reynolds numbers. AIAA Paper No. 87-1266.
Darekar, R.M., Sherwin, S.J., 2001. Flow past a square-section cylinder with a wavy stagnation face. Journal of Fluid Mechanics 426, 263–295.
Gerrard, J.H., 1978. The wakes of cylindrical bluff bodies at low Reynolds number. Philosophical Transactions of the Royal Society of London, Series A 288, 351–382.
Hama, F.R., 1957. Three-dimensional vortex pattern behind a circular cylinder. Journal of Aeronautical Sciences 24, 156–161.
Hunt, J.C.R., Abell, C.J., Paterka, J.A., Woo, H., 1978. Kinematical studies of the flows around free or surface mounted obstacles. Journal of Fluid Mechanics 86, 179–200.
Hayakawa, M., Hussain, F., 1989. Three-dimensionality of organized structures in a plane turbulent wake. Journal of Fluid Mechanics 206, 375–404.
Lasheras, J.C., Choi, H., 1988. Three-dimensional instability of a plane free shear layer: an experimental study of the formation and evolution of streamwise vortices. Journal of Fluid Mechanics 189, 53–86.
Maskel, E.C., 1955. Flow separation in three dimensions. RAE, Report no. AERO 2565.
McLeod, A.R., 1918. On the action of wind on flexible cables with applications to cables towed below aeroplanes and balloon cables. RAE, R&M 554.
Meiburg, E., Lasheras, J.C., 1988. Experimental and numerical investigation of three-dimensional transition in plane wakes. Journal of Fluid Mechanics 188, 1–37.
Owen, J.C., Bearman, P.W., Szewczky, A.A., 2001. Passive control of VIV with drag reduction. Journal of Fluids and Structures 15, 597–605.
Perry, A.E., Fairlie, B.D., 1974. Critical points in flow patterns. Advances in Geophysics B 18, 299–315.
Philips, W.H., 1949. Theoretical analysis of oscillations of a towed cable. NACA TN 1796.
Ramaprian, B.R., Patel, V.C., Sastry, M.S., 1982. The symmetric turbulent wake of a flat plate. AIAA Journal 20, 1228–1235.
Ramberg, S., Griffin, O., 1976. The effects of vortex coherence, spacing, and circulation on the flow-induced forces on vibrating cables and bluff structures. Naval Research Laboratory Technical Report 7945.
Ramberg, S.E., 1983. The effect of yaw and finite length upon the vortex wakes of stationary and vibrating circular cylinders. Journal of Fluid Mechanics 128, 81–107.
Relf, E.F., Powell, C.H., 1917. Tests on smooth and stranded wires inclined to the wind direction, and a comparison of results on stranded wires in air and water. ARC, R&M 307.
Roshko, A., 1954. On the development of turbulent wakes from vortex streets. NACA Report 1191.
Roshko, A., 1961. Experiments on the flow past a circular cylinder at very high Reynolds number. Journal of Fluid Mechanics 10, 345–361.
Sears, W.R., 1948. Boundary layers of yawed cylinders. Journal of Aeronautical Sciences 15, 491–496.
Shirakashi, M., Hasegawa, A., Wakiya, S., 1986. Effect of secondary flow on Karman vortex shedding. Bulletin of the Japan Society of Mechanical Engineers 29 (250), 1124–1129.
Sreenivasan, K.R., 1981. Approach to self preservation in plane turbulent wakes. AIAA Journal 19, 1365–1367.
Surry, J., 1965. Experimental investigation of the characteristics of flow about curved circular cylinders, University of Toronto, UTIAS Technical Note 89.
Thomson, K.D., Morrison, D.F., 1971. The spacing, position and strength of vortices in the wake of slender cylindrical bodies at large incidence. Journal of Fluid Mechanics 50, 751–783.
Tobak, M., Peake, D.J., 1982. Topology of three-dimensional separated flows. Annual Review of Fluid Mechanics 14, 61–85.
Townsend, A.A., 1979. Flow patterns of large eddies in a wake and in a boundary layer. Journal of Fluid Mechanics 95, 515–527.
Wei, T., Smith, C.R., 1986. Secondary vortices in the wake of circular cylinders. Journal of Fluid Mechanics 169, 513–533.
Williamson, C.H.K., 1996. Three dimensional wake transition. Journal of Fluid Mechanics 328, 345–407.